JOURNAL OF MAGNETIC RESONANCE **124,** 61–71 (1997)
ARTICLE NO. MN967482

The Influence of a Scalar-Coupled Deuterium upon the Relaxation of a ^{15}N Nucleus and Its Possible Exploitation as a Probe for Side-Chain Interactions in Proteins

JONATHAN BOYD, TAPAS K. MAL, NICK SOFFE, AND IAIN D. CAMPBELL

Department of Biochemistry and Oxford Centre for Molecular Sciences, South Parks Road, University of Oxford, Oxford, OX1 3QU, United Kingdom

Received June 24, 1996; revised September 11, 1996

The magnitude of the quadrupole coupling constant ($e^2Qq/\hbar$) of a deuteron is a good probe for hydrogen bonding. In protein structures, hydrogen-bonding interactions between side chains, between side chains and ligands, and between side chains and solvent are frequently found. An experiment that detects, via scalar coupling, the influence of a deuteron on the ^{15}N nucleus of asparagine or glutamine side chains is presented. The experiment depends upon the resolution of the $^1\Delta^{15}$N(D) isotope shifts that allow the various isotopomers and isotopologues to be distinguished when ^{15}N-labeled samples are dissolved in solvent mixtures of H_2O/D_2O. ^{15}N lineshapes with theoretical simulations that provide estimates for the ^{2}H quadrupole coupling constants are presented. The influence of ^{15}N–^{2}H dipolar–quadrupole cross correlation and the resulting small frequency shifts in the ^{15}N multiplet are resolved in some of the spectra. The experimental data are provided using the free amino acids asparagine and glutamine for which the side chains were isotopically enriched in ^{15}N and the recombinant pair of modules, fibronectin type 1 and epidermal growth factor, (F1-G) of tissue plasminogen activator, which were uniformly isotopically enriched in ^{15}N. © 1997 Academic Press

INTRODUCTION

Most ^{15}N isotopically enriched recombinant proteins will contain several amino acids whose side chains also have a ^{15}N nucleus. There are several recent NMR structures which highlight possible interesting hydrogen-bonding or salt bridge interactions involving amino acids with ^{15}N nuclei in their side chains. These recent examples include hydrogen-bond interactions between side chains in model peptides (*1*) and between protein side chains and bound ligands (*2–5*).

NMR has been used extensively to probe hydrogen bonds in solution (*6*). The measurement of primary isotope shifts which arise from substitution of a ^{2}H or ^{3}H for a hydrogen-bonded proton can be used to give precise information on the symmetry of the hydrogen bond. The magnitude and sign of the primary isotope shift has been shown to give information about the shape of the hydrogen-bond potential-energy surface (*7, 8*). A method for predicting hydrogen-bond lengths, which is applicable to the backbone amide protons in proteins, has also been described (*9, 10*). This technique involves a measurement of the difference between the observed amide proton chemical shift and its random coil chemical shift. The observed difference can then be related to the length of the hydrogen bond.

For a hydrogen bond of the form X–^{2}H···Y, the magnitude of the deuterium quadrupole coupling constant ($e^2Qq/\hbar$) has been correlated with the strength of hydrogen bonding. Theoretical (*11, 12*) and experimental evidence for this relationship has been given. The experimental data have been obtained mainly by using solid-state NMR and NQR techniques (*13–19*), but there have also been investigations in the liquid phase (*20–22*). It seems to be the difference between bond length of X–^{2}H and ^{2}H···Y that determines the value of the deuterium quadrupole coupling constant (*11, 13, 17*). As the hydrogen-bond strength increases, the X–^{2}H bond length increases and the contribution of the X nucleus to the electric field gradient at the ^{2}H nucleus decreases faster than the additional contribution arising from the more distant charge distribution represented by the Y atom (*11*). Very good correlations of the ^{2}H quadrupole coupling constant have also been found with either $(^2\text{H}\cdots\text{Y})^{-3}$ (*15, 16*) or $(^2\text{H}\cdots\text{Y})^{-1}$ (*18*) as well as with the difference $[(\text{X}-^2\text{H}) - (^2\text{H}\cdots\text{Y})]$. All these relationships predict a decrease of the net field gradient with increasing strength of the hydrogen bond. Most of the published data have been concerned with the O–^{2}H···O system. However, similar arguments have been applied to the N–^{2}H···Y system, where the ^{2}H quadrupole coupling constant has been found to exhibit a large variation in magnitude because of the influence of hydrogen bonding (*15, 19*).

To estimate the ^{2}H quadrupole coupling constant in a macromolecule in solution, we have used an experiment which observes, indirectly, the environment of a deuterium nucleus through its influence upon the relaxation of a ^{15}N

1090-7807/97 $25.00

nucleus to which it is scalar coupled. The experiment depends primarily upon the resolution of the fairly large $^1\Delta^{15}N(D)$ isotope shifts[1] when a sample, containing asparagine or glutamine, is dissolved in a solvent mixture comprising H_2O and D_2O. Theoretical simulations of the resulting ^{15}N lineshapes require a number of broad assumptions but do yield estimates of the magnitude of the ^2H quadrupole coupling constant both in the free amino acids and when these residues are part of a protein. An important assumption is that the interactions responsible for the tertiary protein structure, some of which are hydrogen bonds, are not significantly altered by the solvent mixture. This requires that the strength of a particular hydrogen bond should remain essentially independent of the solvent ratio.

THEORY

The system to be investigated here comprises three spins, ^{15}N, ^1H, and ^2H. However, during the ^{15}N evolution period of a 2D $^{15}N-^1H$ correlated experiment, the scalar coupling between the ^{15}N and ^1H nuclei is removed by ^1H broadband decoupling, reducing the ^{15}N resonance to a three-line multiplet. The relaxation of a spin-$\frac{1}{2}$ nucleus scalar coupled to a spin-1 nucleus has been described (*23–31*). Perhaps the most striking feature of this spin system has been shown to arise from the dipolar–quadrupolar cross-correlation interaction. For a spin-$\frac{1}{2}$ three-line multiplet, this relaxation process can give rise, in medium-sized molecules such as proteins, to quite large frequency shifts for the individual components of a multiplet, leading to very asymmetric lineshapes (*28–31*).

The labels, eigenstates and eigenvalues for a $^{15}N-^2H$ scalar-coupled spin system, where J_{ND} is negative, are $|1\rangle = |\alpha+\rangle = (\upsilon_N - J_{ND})/2 + \upsilon_D$, $|2\rangle = |\alpha 0\rangle = \upsilon_N/2$, $|3\rangle = |\alpha-\rangle = (\upsilon_N + J_{ND})/2 - \upsilon_D$, $|4\rangle = |\beta+\rangle = -(\upsilon_N - J_{ND})/2 + \upsilon_D$, $|5\rangle = |\beta 0\rangle = -\upsilon_N/2$, $|6\rangle = |\beta-\rangle = -(\upsilon_N + J_{ND})/2 - \upsilon_D$, where α, β and $+$, 0, $-$ refer to the spin states of the ^{15}N and ^2H nuclei, respectively.

The matrix elements, transitions and characteristic frequencies (rads/sec) required for the three $p = +1$ ^{15}N single-quantum coherences associated with the $+$, 0, $-$ spin states of the deuteron, expressed in terms of single-transition operators, are $\rho_{14}^{+} = |\alpha+\rangle\langle\beta+| = \omega_N^{+} = \Omega_N - 2\pi J_{ND}$, $\rho_{25}^{0} = |\alpha 0\rangle\langle\beta 0| = \omega_N^{0} = \Omega_N$, $\rho_{36}^{-} = |\alpha-\rangle\langle\beta-| = \omega_N^{-} = \Omega_N + 2\pi J_{ND}$, where ω_N is the Lamor frequency of spin N (in a frame of reference rotating at the carrier frequency ω_{rf}) with offset $\Omega_N = \omega_N - \omega_{rf}$. Consequently, with $2\pi J_{ND}$ negative (and $> |\delta|$), the relative transition frequencies associated with the single-transition operators are in the order $\rho_{14}^{+}(\omega_N^{+}) > \rho_{25}^{0}(\omega_N^{0}) > \rho_{36}^{-}(\omega_N^{-})$.

The time evolution of the density matrix can be described by (*24*)

$$d\{\sigma(t)\}/dt = -\{iH_0 + \mathbf{\Gamma}\}\{\sigma(t)\}, \qquad [1]$$

where H_0 is the nuclear spin superoperator and $\mathbf{\Gamma}$ is the relaxation superoperator. The diagonal elements of H_0 for the $^{15}N-^2H$ spin system contain information about the spin variables such as resonance offset (Ω) and scalar coupling constant (J_{ND}), as well as the dynamic frequency shifts (δ) arising from relaxation (*28, 29*).

The main relaxation mechanisms contributing to ^{15}N relaxation are quadrupole relaxation of the ^2H nucleus, dipole–dipole relaxation of both the $^{15}N-^1H$ and $^{15}N-^2H$ spin pairs, and anisotropic chemical-shift relaxation of the ^{15}N and possibly ^2H nuclei. These relaxation mechanisms can give rise to several cross-correlation phenomena; these include dipolar–quadrupole ($^{15}N-^2H$, ^2H), csa–quadrupole (^2H, ^2H), and dipolar–csa ($^{15}N-^2H$, ^{15}N). The dipolar cross-correlation process ($^{15}N-^1H$, $^{15}N-^2H$) was assumed to be small and was neglected. A chemical-exchange term, which is less well defined than those discussed above, could also give rise to ^{15}N line broadening. This last process would reflect a fairly slow motion of the complete side chain between several well-populated sites at a rate which is still fast enough to average any ^{15}N chemical-shift differences.

The frequency properties of the correlation function are developed using the spectral-density function defined as

$$\begin{aligned} j(a\omega) &= (1/4\pi)\tau_r/[1 + i(a\omega)\tau_r] \qquad [2] \\ &= (1/4\pi)[J(a\omega) - iQ(a\omega)], \end{aligned}$$

where $J(a\omega)$ and $Q(a\omega)$ are the real and imaginary terms of the complex spectral density, $j(a\omega)$ (*24, 28, 29, 34*). It has been shown (*24, 35*) that the significance of the imaginary term of the spectral density, if nonzero, is to produce a small frequency shift, δ, the magnitude of which is dependent on the motional properties of the spins. The correlation function is subdivided following the approach of Lipari and Szabo (*36*). In this case, the spectral density is of the form $j(a\omega) = (1/4\pi)\{S^2\tau_r/[1 + i(a\omega)\tau_r] + (1 - S^2)\tau/[1 + i(a\omega)\tau]\}$, where τ_r is the isotropic rotational correlation time and $1/\tau = 1/\tau_r + 1/\tau_i$, τ_i is the effective correlation time characterizing the rapid internal motions (where $\tau_i \ll \tau_r$), and S^2 is an order parameter. A justification for this expansion, in the presence of both auto- and cross-correlated motions, is given later.

The 3×3 matrix, $\mathbf{\Gamma}$, is formed through summation of

[1] The definition, $^n\Delta X(^1H, ^2H) = {}^n\Delta X(D) = \delta X(^1H) - \delta X(^2H)$, which is used for the isotope shifts follows that in Ref. (*48*), where $\delta X(^2H)$ is the chemical shift of the deuterated species. If the isotope shift is to lower frequency then, with this definition, the sign is positive.

the individual relaxation contributions, where the interaction constants are defined as

$$\text{dipolar, } D_{ij} = (6\pi/5)^{1/2}(\mu_0/4\pi)\gamma_i\gamma_j\hbar/r_{ij}^3;$$

$$\text{csa, } C_i = (8\pi/15)^{1/2}\gamma_i\Delta\sigma_i B_0;$$

$$\text{quadrupolar, } Q_D = (3\pi/40)^{1/2}(e^2Qq/\hbar).$$

The matrix $\mathbf{\Gamma} = \Sigma_{i=1,8}\,\mathbf{\Gamma}^i$, where $\mathbf{\Gamma}^1$ is the contribution to relaxation from ^{2}H quadrupolar relaxation, $\mathbf{\Gamma}^2$ is a possible contribution to relaxation from ^{2}H csa–quadrupole cross correlation, $\mathbf{\Gamma}^3$ is the contribution to relaxation from ^{15}N–^{2}H, ^{2}H dipolar–quadrupolar cross correlation, $\mathbf{\Gamma}^4$ and $\mathbf{\Gamma}^5$ are the contributions from ^{15}N–^{1}H and ^{15}N–^{2}H dipolar relaxation respectively, $\mathbf{\Gamma}^6$ is the contribution to relaxation from ^{15}N csa, $\mathbf{\Gamma}^7$ is the contribution to relaxation from ^{15}N–^{2}H, ^{15}N dipolar–csa cross correlation, and $\mathbf{\Gamma}^8$ is a possible contribution to relaxation from chemical exchange.

The individual relaxation elements of the relaxation matrix, $\mathbf{\Gamma}$, for each relaxation mechanism are given below, where the superscript is used to denote the particular relaxation mechanism and the subscript identifies the matrix element:

$\mathbf{\Gamma}^1$: $\Gamma^1_{1414} = \Gamma^1_{3636} = 4(Q_D)^2(1 + \eta^2/3)\{J(\omega_D) + 2J(2\omega_D)\}$;

$-0.5\Gamma^1_{2525} = \Gamma^1_{1425} = \Gamma^1_{2514} = \Gamma^1_{2536} = \Gamma^1_{3625} = -4(Q_D)^2(1 + \eta^2/3)\{J(\omega_D)\}$;

$\Gamma^1_{1436} = \Gamma^1_{3614} = -8(Q_D)^2(1 + \eta^2/3)\{J(2\omega_D)\}$, where η is the asymmetry parameter of the ^{2}H electric-field-gradient tensor. η for ^{2}H is usually small and axial symmetry is a good assumption for a N–D spin system.

$\mathbf{\Gamma}^2$: $\Gamma^2_{1414} = -\Gamma^2_{1425} = -\Gamma^2_{2514} = \Gamma^2_{2536} = \Gamma^2_{3625} = -\Gamma^2_{3636} = 4(Q_DC_D)P_2\cos(\theta_{QC})J(\omega_D)$, where $P_2\cos(\theta_{QC})$ is the second-order Legendre polynomial and θ_{QC} is the angle between the principal components of the assumed axially symmetric electric-field-gradient and chemical-shift tensors of the deuteron. This relaxation mechanism does not contribute to the dynamic frequency shift (*28*). Values for the ^{2}H chemical-shift anisotropy, $\Delta\sigma_D$, of a ND spin system are in the range of -14 ppm (*37*). This magnitude is too small for line broadening from the cross-correlation process to be discernible in the experimental spectra reported here, and the contribution of this mechanism to relaxation was neglected.

$\mathbf{\Gamma}^3$: $\delta^3_{14} = -0.5\delta^3_{25} = \delta^3_{36} = -4(Q_DD_{ND})P_2\cos(\theta_{QD})Q(\omega_D)$, where $P_2\cos(\theta_{QD})$ is the second-order Legendre polynomial and θ_{QD} is the angle between the ND internuclear vector and the principal component of the assumed axially symmetric electric-field-gradient tensor of the deuteron. $Q(\omega_D)$ refers to the imaginary term of the complex spectral density. The maximum magnitude of the dynamic frequency shift, δ^3_{25}, was found from the simulations to be 1.7 Hz.

$\mathbf{\Gamma}^4$: $\Gamma^4_{1414} = \Gamma^4_{2525} = \Gamma^4_{3636} = (D_{NH})^2\{2J(0)/3 + J(\omega_H - \omega_N)/6 + 0.5J(\omega_N) + J(\omega_H) + J(\omega_N + \omega_H)\}$;

$\delta^4_{14} = \delta^4_{25} = \delta^4_{36} = (D_{NH})^2\{Q(\omega_H\text{-}\omega_N)/6 + 0.5Q(\omega_N) + Q(\omega_H + \omega_N)\}$, where $Q(a\omega)$ refers to the imaginary term of the complex spectral density.

$\mathbf{\Gamma}^5$: $\Gamma^5_{1414} = \Gamma^5_{3636} = (D_{ND})^2\{8J(0)/3 + J(\omega_D - \omega_N)/3 + 2J(\omega_N) + J(\omega_D) + 2J(\omega_N + \omega_D)\}$;

$\Gamma^5_{2525} = (D_{ND})^2\{2J(\omega_D - \omega_N)/3 + 2J(\omega_D) + 4J(\omega_N + \omega_D)\}$;

$\Gamma^5_{1425} = \Gamma^5_{2514} = \Gamma^5_{2536} = \Gamma^5_{3625} = (D_{ND})^2\{J(\omega_D)\}$;

$\delta^5_{14} = \delta^5_{36} = (D_{ND})^2\{Q(\omega_D - \omega_N)/3 + 2Q(\omega_N) + 2Q(\omega_D + \omega_N)\}$;

$\delta^5_{25} = (D_{ND})^2\{2Q(\omega_D - \omega_N)/3 + 4Q(\omega_D + \omega_N)\}$, where $Q(a\omega)$ refers to the imaginary term of the complex spectral density. The maximum dynamic frequency shift, δ^5, from this mechanism is in all the cases considered here $<8\%$ of the magnitude of the contribution to the dynamic frequency shift from δ^3, the dipolar–quadrupolar cross-correlation mechanism.

$\mathbf{\Gamma}^6$: $\Gamma^6_{1414} = \Gamma^6_{2525} = \Gamma^6_{3636} = (C_N)^2\{2J(0)/3 + 0.5J(\omega_N)\}$, where the ^{15}N chemical-shift tensor for the side-chain amide of asparagine has been found to be axially symmetric to a good approximation $(1 + \eta^2/3) = 1.05$, and with $\Delta\sigma_N = -165$ ppm (*38*); this value for $\Delta\sigma_N$ was also used for simulations involving glutamine.

$\mathbf{\Gamma}^7$: $\Gamma^7_{1414} = -\Gamma^7_{3636} = (D_{ND}C_N)P_2\cos(\theta_{DC})\{8J(0)/3 + 2J(\omega_N)\}$;

$\delta^7_{14} = -\delta^7_{36} = (D_{ND}C_N)P_2\cos(\theta_{DC})\{2Q(\omega_N)\}$, where $P_2\cos(\theta_{DC})$ is the second-order Legendre polynomial and θ_{DC} is the angle between the ^{15}ND internuclear vector and the principal component of the axially symmetric ^{15}N chemical-shift tensor and $Q(\omega_N)$ refers to the imaginary term of the complex spectral density. The principal component of the ^{15}N csa tensor lies in the same plane as the ND internuclear vector but is not collinear with it, subtending an angle of 30° (or 150°). A comment about the approximate error introduced into the simulations by assuming collinearity for either of the Z-1-d or E-1-d isotopomers appears later. The maximum magnitude of the dynamic frequency shift, δ^7, was found from the simulations to be about 0.1 Hz. Using negative values for J_{ND} and $\Delta\sigma_N$ results in line broadening for the low-frequency component of the ^{15}N multiplet.

$\mathbf{\Gamma}^8$: $\Gamma^8_{1414} = \Gamma^8_{2525} = \Gamma^8_{3636} = R_{ex}$, where R_{ex} is an exchange contribution to the ^{15}N relaxation.

The complex eigenvalues and eigenvectors of Eq. [1] were obtained using NAG library routines (NAG Group Ltd., Oxford, UK).

EXPERIMENTAL

The samples of ^{15}N-labeled asparagine and glutamine were used without further purification. The structure of the ^{15}N isotopically labeled recombinant protein sample of fi-

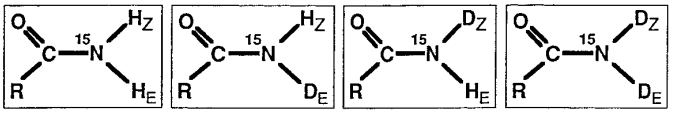

FIG. 1. The nomenclature for each species follows that in Ref. (*43*), where E-1-d and Z-1-d are referred to as isotopomers and the other two species are called isotopologues.

bronectin type 1 and epidermal-growth-factor-like pair of modules (F1-G) of tissue plasminogen activator, at pH 3, has been reported (*39, 40*). All NMR spectra were recorded from samples at pH 3 and 10°C. A temperature of 10°C was chosen in order to reduce the rate of intermolecular solvent exchange. Using the data supplied in (*41*), this rate was calculated to be about 0.2 s^{-1} for a fully exposed asparagine or glutamine at pH 3 in H_2O. The pH values reported are the direct meter readings, uncorrected for isotope effects.

The NMR spectra were obtained on a homebuilt spectrometer, operating at 750 MHz for ^1H, which was interfaced to an Oxford Instruments superconducting magnet and which used a homemade RF probehead (*42*) with a three-axis gradient set.

The lock gating circuitry incorporated a fast GaAs RF switch which enabled the probe lock coil to be connected to the ^2H lock or to the output of the ^2H decoupler. This enabled interleaving of the decoupling while retaining normal lock mode operation for long-term experiments. The switch has a very low insertion loss, ensuring that the lock sensitivity is not degraded.

The chemical-shift range of the deuterons to be decoupled was fairly small, approximately ±85 Hz. A WALTZ16 RF field strength of $\gamma B_1/2\pi = 350$ Hz was found to be sufficient; this RF field strength also significantly exceeds J_{ND} and typically it was found that (*31*) $[\gamma B_1 T_1(^2H)]^2 \gg 1$ where $T_1(^2H)$ was estimated from the lineshape simulations.

The primary isotope shift, $^1\Delta H(D)$, was measured using the solvent HOD signal as a reference. Any additional contribution to the measured primary isotope shift of the amino acid from an isotope shift in the HOD resonance was neglected. These ^1H and ^2H spectra were recorded unlocked.

RESULTS AND DISCUSSION

There are four distinct species, differing in the side-chain amide group, when a sample of asparagine or glutamine is dissolved in a solvent mixture of H_2O and D_2O, as shown in Fig. 1. Provided there are no isotope effects on the chemical equilibria (see text) the relative proportions of each species present in the solution can be estimated from the molar ratio of the solvent with a value of 3.85 for K_W (*44, 45*), where $K_W = 4[HOD]^2/[D_2O][H_2O]$. K_W does not vary significantly with temperature (*46*). Using a value for K_W of 4 changes the $[HOD]/[H_2O]$ ratio by only about 1%. This is inside the anticipated experimental errors of the NMR integrals and a value for K_W of 4 was assumed.

A part of the ^{15}N scalar-coupled 750 MHz one-dimensional ^1H NMR spectrum from a sample of the amino acid glutamine, ^{15}N-labeled in the side-chain amide group, is shown in Fig. 2. It is usual for the H_E (trans) proton to be downfield of the H_Z (cis) proton in primary amides (*47*), and this observation makes possible the assignment of the protons H_E and H_Z in the free amino acid. The two-bond, $^2\Delta H(D)$, isotope effect of ^2H substitution is clearly distinguished. The shift is to higher frequency for both the Z-1-d and E-1-d isotopomers and is largest for the E-1-d isotopomer. The substitution of a lighter isotope by a heavy isotope usually leads to a shift to a lower frequency (*48*). However, for the ammonium ion, substitution of ^1H by ^2H causes a shift of the ^1H resonances to a higher frequency (*49*); a possible explanation for this observation, based upon the electronegativity of the nitrogen, has been provided (*50*).

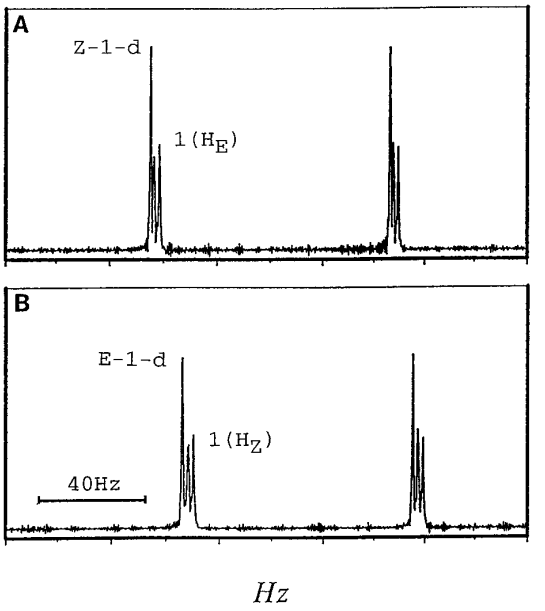

FIG. 2. The spectrum was recorded from a sample of glutamine ^{15}N-enriched in the side-chain amide dissolved in an equimolar mixture of H_2O/D_2O. (A) $^{15}N-^1H$ scalar-coupled resonances from species $1(H_E)$ and Z-1-d and (B) $^{15}N-^1H$ scalar-coupled resonances from species $1(H_Z)$ and E-1-d. The spectrum, recorded without ^{15}N decoupling, has a final digital resolution of 0.19 Hz/pt, the major and minor tick marks are at 40 and 20 Hz, respectively, and the time-domain data were apodized with a Lorenztian-to-Gaussian resolution-enhancement function prior to Fourier transformation. The chemical-shift difference between the resonances of $1(H_E)$ and $1(H_Z)$ is 565 Hz (0.753 ppm), $JH_ZH_E = 2.0$ Hz, $J^{15}NH_Z = -89.3$ Hz, $J^{15}NH_E = -91.2$ Hz, and the J_{HD} coupling constant could not be resolved. The two-bond isotope shifts, $^2\Delta H(D)$, are -2.2 Hz (-2.93×10^{-3} ppm) and -3.0 Hz (-4.0×10^{-3} ppm) for the Z-1-d and E-1-d isotopomers respectively.

Whether a similar consideration applies to glutamine (or to asparagine which exhibits similar shifts) is not known. We note that the isotope shift $^1\Delta H(^{14}N, ^{15}N)$, measured using an equimolar mixture and ^{14}N decoupling, is <1 Hz for both ^1H resonances. The chemical exchange via the solvent between the various species at this pH and temperature is clearly very slow as no significant broadening of the resonances is observed [$k_{ex} \ll |2\pi(^2\Delta H(D))|$].

In the absence of isotope effects on the chemical equilibrium, the relative proportions of the various species, $^{15}NH_2$, ^{15}NHD, and $^{15}ND_2$, are given by the statistical formulas d^2, $2d[1-d]$, $[1-d]^2$, respectively, where d is the mole fraction of H_2O in the solvent. To measure the integrals from this sample, a 1D ^1H spectrum was recorded using a binomial excitation sequence, avoiding solvent saturation, with a recycle delay of 30 s. For each isotopomer, including a fairly large experimental error of about 10%, the integrals, derived from curve fitting Lorentzian lines to the spectrum, indicate a deviation from the statistical proportions. The isotope exchange equilibrium constants, defined as $\varphi_E = (^{15}NH_ED/^{15}NH_EH_Z)(d/[1-d])$ and $\varphi_Z = (^{15}NDH_Z/^{15}NH_EH_Z)(d/[1-d])$, were found to be 0.72 ± 0.1 and 0.79 ± 0.11 respectively. The other isotope exchange equilibria, represented by $\varphi = (^{15}ND_2/^{15}NHD)(d/[1-d])$, cannot be measured from these spectra.

There are many reported examples, including proteins, which exhibit isotope exchange equilibrium constants (fractionation factors) different from unity (*46, 48, 51*). A value for φ less than unity indicates that both isotopomers have a preference for ^1H over ^2H, suggesting both protons are involved in hydrogen bonds either with the solvent or perhaps in some intramolecular interaction with the carboxyl group. If the amino acid is changed to asparagine, the chemical-shift characteristics of the ^1H spectrum are similar at this pH and temperature.

Measurement of the primary isotope shift, $^1\Delta H(D)$, from either asparagine or glutamine for either the H_Z or the H_E site indicates that the shifts are positive and with a magnitude of less than 0.03 ppm. The observation of a primary isotope shift which is in each case positive and close to zero is consistent with hydrogen bonds which may be described by a double-well potential energy surface where the equilibrium position of the two isotopes is similar (*7, 8*).

A one-dimensional ^2H spectrum of a sample of asparagine in D_2O is shown in Fig. 3A. The most striking feature of this spectrum is the large difference in linewidth for the ^2H resonances. The linewidth for the D_Z deuteron is significantly larger than that observed for the D_E deuteron. ^2H inversion-recovery curves for these resonances are shown in Fig. 3B. The ^2H longitudinal relaxation times are also different and are found to have values closely similar to the ^2H T_2 values derived from curve fitting Lorentzian lines to the spectrum in Fig. 3A.

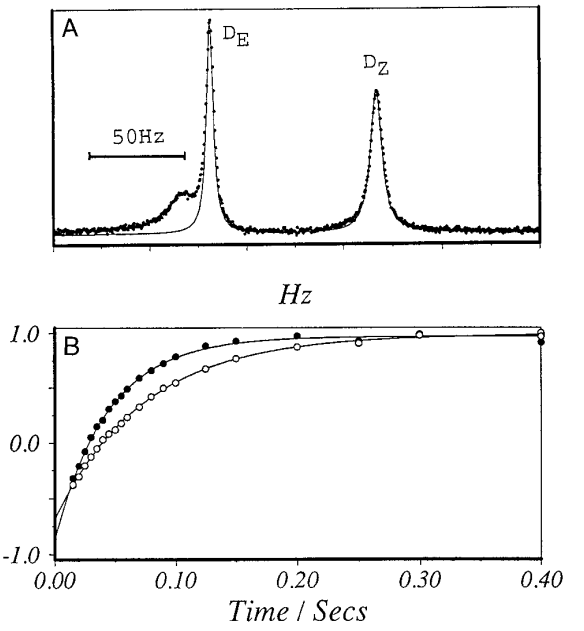

FIG. 3. (A) One-dimensional ^2H spectrum recorded at 115.1 MHz, with broadband WALTZ-16 ^{15}N decoupling, from a sample of asparagine dissolved in D_2O. The solid line represents the sum of two simulated Lorentzian lineshapes, with a T_2 of 44.9 ms for D_Z and 75 ms for D_E. The broad peak to high frequency of the ^2H D_E resonance is assigned to the $^{14}ND_3$ group. The major and minor tick marks are at 50 and 25 Hz, respectively. (B) ^2H longitudinal inversion-recovery data for the deuterons D_Z (filled circles) and D_E (open circles) recorded at 115.1 MHz. The ^2H T_1 values were found to be 44.9 and 75.3 ms for the D_Z and D_E resonances, respectively. The three-parameter curve fitting used a function of the form $A\{1-(W+1)e^{-t/T_1}\}$ to estimate the ^2H T_1 values.

In the extreme-narrowing regime, assuming the only significant mechanism contributing to ^2H relaxation is that arising from fluctuations of the nuclear quadrupole moment, $R_1 = R_2 = 20\,Q_D^2\,(1+\eta^2/3)J(0) = 3\pi/2(e^2Qq/\hbar)^2(1+\eta^2/3)J(0)$ (*24*) where η, the asymmetry parameter, is defined as a positive quantity with a value between 0 and 1. The asymmetry parameter for ^2H is usually small (*52*) and the principal component of the electric-field-gradient tensor for a ND group has been shown to lie along or very close to the bond (*52*). In the discussion which follows, we assume that η is sufficiently small that it can be neglected in the determination of values for $e^2Qq/\hbar$. The sign of $e^2Qq/\hbar$ cannot be determined from these data but could be important in the dipolar-quadrupolar cross-correlation process to be considered later. With these assumptions, the probable basis for the ^2H relaxation behavior is a different magnitude of $e^2Qq/\hbar$ for the D_E and D_Z deuterons.

To act as a restraint on the motional parameters chosen to model the ^2H relaxation data, ^{15}N T_1 and $^{15}N-^1H$ NOE time-development data were recorded from a sample of as-

paragine in H_2O, Fig. 4. The major contribution to ^{15}N longitudinal relaxation is the $^{15}N-{}^{1}H$ dipole–dipole mechanism for each proton with a small contribution from ^{15}N chemical-shift anisotropy. Anticipating a model of isotropic motion, which is justified later, in the extreme-narrowing regime, $R_1 = \rho_N = (10/3D_{NH}^2 + C_N^2)J(0) + \rho^*$, where ρ^* is used to indicate small contributions to ^{15}N relaxation from other mechanisms such as trace paramagnetic impurities. Contributions to relaxation from the $^{15}N-{}^{1}H$, ^{15}N dipolar–csa cross-correlation process were experimentally removed (*53*), and the $^{15}N-{}^{1}H$ dipole–dipole cross-correlation term is small and can be neglected.

^{15}N deuterium-coupled spectra from the Z-1-d and E-1-d isotopomers of the sample of asparagine in a H_2O/D_2O solvent mixture are shown in Fig. 5B. These data were recorded using the pulse sequence shown in Fig. 5A and clearly show that the ^{15}N lineshape for each isotopomer is different, reflecting the distinctive contributions to ^{15}N transverse relaxation from the scalar coupling to the ^{2}H nuclei. These spectra also show that the $^{1}\Delta^{15}N(D)$ isotope shift for each isotopomer is different and is measured, relative to the $^{15}NH_2$ group, to be 35.7 Hz (0.47 ppm) and 39.9 Hz (0.525 ppm) for the Z-1-d and E-1-d isotopomers, respectively. The isotope shift of the broad ^{15}N resonance from the $^{15}ND_2$ deuterium-coupled isotopologue, observed by ^{15}N direct detection

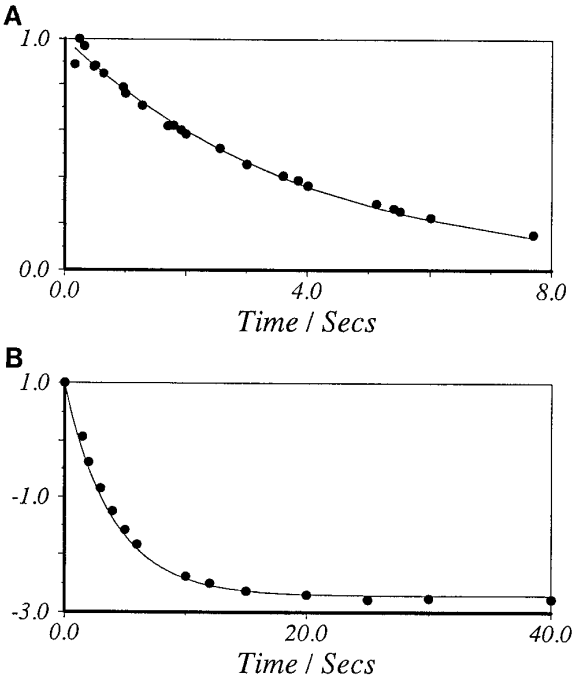

FIG. 4. (A) ^{15}N longitudinal-relaxation data recorded at 76 MHz, using a pulse sequence previously described (*54*), for a sample of asparagine, ^{15}N-labeled in the side-chain amide, dissolved in H_2O. The data are plotted as intensity versus the relaxation delay. The solid curve is a single-exponential fit to the data with a rate constant, $\rho_N = 0.255\ s^{-1}$. (B) $^{15}N-{}^{1}H$ NOE time-development curve. The data are plotted as intensity versus the ^{1}H RF saturation period. A recycle delay of 40 s was used. The solid curve follows an equation of the form $\{[(1 - X)e^{-\rho_N t}] + X\}$, where $X = \{1 + \gamma_H/\gamma_N(2\sigma_{NH}/\rho_N)\}$, $\rho_N = 0.255\ s^{-1}$ and $\sigma_{NH} = 0.048\ s^{-1}$.

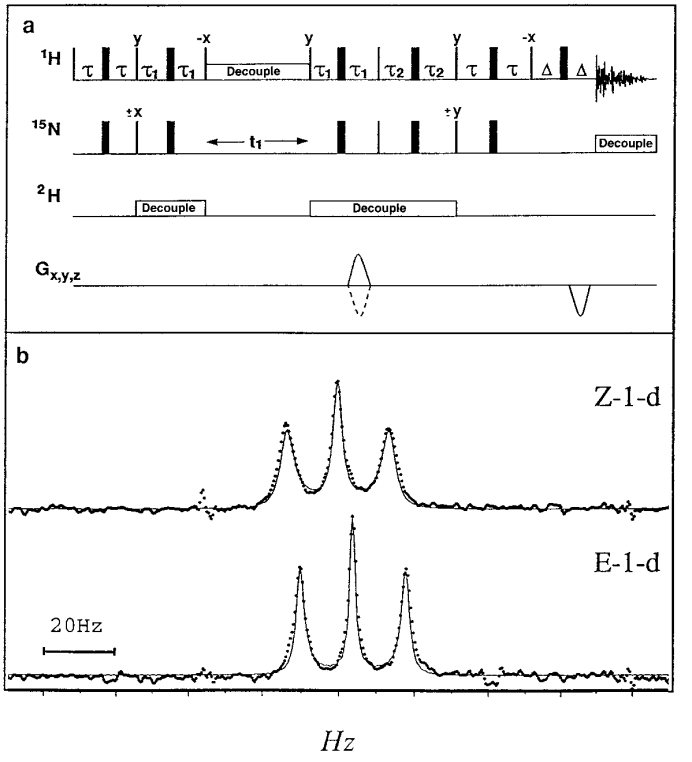

FIG. 5. (A) The RF pulse sequence used to record the ^{15}N- ^{1}H-correlated data. This pulse sequence follows closely those described in Refs. (*57, 58*). ^{2}H decoupling is applied during all preparation periods when ^{15}N coherence is evolving to reduce differential relaxation of the individual ^{15}N multiplets. Signals from the $^{15}NH_2$ groups were suppressed by choosing $\tau_1 = 1/4J_{NH}$. ^{2}H decoupling is used only during the intervals shown but the lock receiver, which is blanked during periods of decoupling, was not reopened until after acquisition was complete. Under the influence of the ^{2}H scalar coupling, and in the presence of ^{1}H decoupling, the evolution of the ^{15}N in-phase coherence (I^+) during the t_1 evolution period is described by

$$I^+ \rightarrow I^+ \cos(\omega_N t_1)\{1 + S_z^2[\cos(2\pi J_{ND} t_1) - 1]\} + I^+ S_z \cos(\omega_N t_1)\sin(2\pi J_{ND} t_1).$$

(B) Experimental cross sections recorded at 76 MHz, from a sample of asparagine dissolved in an equimolar mixture of H_2O/D_2O, parallel to F_1 at the ^{15}N frequency corresponding to the ^{1}H resonances from the isotopomers Z-1-d (upper trace) and E-1-d (lower trace). The data were obtained using the pulse sequence in (A), which used ^{1}H broadband Dipsi_3 decoupling during the ^{15}N evolution period. The solid lines are simulations of the experimental data which used the following parameters: $r_{NH} = 0.102$ nm, $r_{ND} = 0.1015$ nm, $B_0 = 17.6$ T, $\Delta\sigma_N = -165$ ppm and $\theta_{QD} = \theta_{DC} = 0$, $J^{15}ND_Z$ −13.7 Hz, and $J^{15}ND_E$ −14 Hz. The time-domain data comprised 512 complex points, dwell time 1250 μs, which were zero filled twice without any apodization prior to Fourier transformation. The major and minor tick marks are at 20 and 10 Hz respectively.

TABLE 1

Rotational Correlation Time, τ_r, and Quadrupole Coupling Constants, $e^2Qq/\hbar$, for the Z-1-d and E-1-d Isotopomers of the Free Amino Acids Asparagine and Glutamine, ^{15}N-Enriched in the Side Chain, from Samples Dissolved in an Equimolar Mixture of H_2O/D_2O, pH 3 and 10°C

	τ_r (ps)	$e^2Qq/\hbar$ (kHz) Z-1-d	$e^2Qq/\hbar$ (kHz) E-1-d
Asparagine	18	290	225
Glutamine	21	290	225
Formamide	5.1	280[a]	230[a]

Note. The data for formamide are taken from (*22*) and were obtained at a temperature of 25°C.

[a] The assignment for the H_Z and H_E resonances was not given in Ref. (*22*), and the allocation to a particular column is arbitrary.

without ^{2}H decoupling (data not shown), is the additive sum of the shifts for the E-1-d and Z-1-d isotopomers to within the digital resolution of the spectrum.

The dipolar interaction vector for ^{15}N longitudinal and transverse relaxation is the ^{15}N–H bond. The principal axis of the assumed axially symmetric ^{2}H electric-field-gradient tensor is assumed to be collinear with this ^{15}N–D internuclear vector (*52*). Chemical-shift anisotropy for ^{2}H was not considered, because the reported values (*37*) are too small to affect the spectra reported here. The axially symmetric ^{15}N csa tensor was assumed to be collinear with either ^{15}N–D bond, although it may make an angle of 30° or 150° (*38*). Neglect of this angle will overestimate the contribution of the (^{15}N–^{2}H, ^{15}N) dipolar-csa cross-correlation relaxation mechanism in those cases where it contributes significantly. For the free amino acids, this relaxation mechanism is quantitatively negligible in comparison to the ^{2}H-quadrupole-induced relaxation. For the protein data, it will cause an overestimation of only about 5% to the total dynamic frequency shift, δ, or <3% to the total relaxation matrix $\mathbf{\Gamma}$. Furthermore, the functions $P_2(\cos\theta_{ab})$ which appear in the spectral density when cross correlations are present (*54*) will reduce, when using the above simplifications, in the limit that $\theta_{QD} = \theta_{DC} = 0$, to the Lipari–Szabo notation where the order parameter S^2 reflects details of the dynamics from processes involving auto and cross correlations.

A possible explanation for the observed relaxation differences (^{2}H and ^{15}N) caused by a deuteron in the D_Z or D_E position could be based on anisotropic rotational diffusion. The degree of anisotropy of the rotational diffusion tensor for a rigid model of asparagine was calculated (*55*) by approximating the structure as a set of nine identical spherical beads, positioned at the coordinates of the heavy atoms of the X-ray structure (*56*). These hydrodynamic calculations of the rotational diffusion tensor show that asparagine may be considered to be axially symmetric and that it is only mildly anisotropic with $D_{\|}/D_{\perp} < 1.5$. However, the free amino acid has significant internal motions associated with the side chain due to changes of the various torsion angles caused by jumps between the potential energy wells. These transitions between potential energy wells, which give rise to averaged $^3J_{HH}$ coupling constants, probably occur on a time scale that approaches the time for rotational diffusion and may contribute to relaxation. In view of these uncertainties, a spherical hydrodynamic model for asparagine was assumed.

The solid line through the data points in Fig. 5B is a simulated spectrum using a rotational correlation time, τ_r, and quadrupole coupling constants shown in Table 1. The parameters also simulate satisfactorily the experimental ^{2}H (T_1 and T_2) and ^{15}N (T_1 and NOE, with $\rho^* = 0.045\ s^{-1}$) relaxation data. Using these parameters, the ^{15}N linewidth is >98% dominated by the ^{2}H quadrupolar-induced relaxation process. The dynamic frequency shift caused by the dipolar-quadrupolar cross-correlation process (<0.1 Hz) is too small to be identifiable in these spectra.

The different values found for the quadrupole coupling constants of the D_Z and D_E deuterons in asparagine are similar in magnitude to those recently reported from liquid formamide (*22*) as seen from Table 1. Within the framework of the relationship between $e^2Qq/\hbar$ and hydrogen-bond strength, these data for the free amino acid would imply

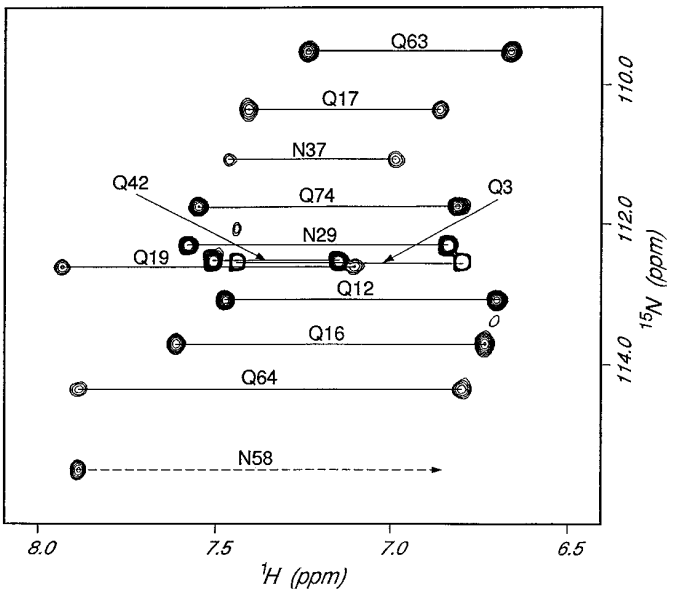

FIG. 6. Part of a two-dimensional ^{15}N–^{1}H correlated data set recorded at 750 MHz from a sample of the protein F1-G at pH 3.0 and 10°C. The assignments for all of the side-chain ^{1}H and ^{15}N resonances of the asparagine and glutamine residues in this protein are indicated.

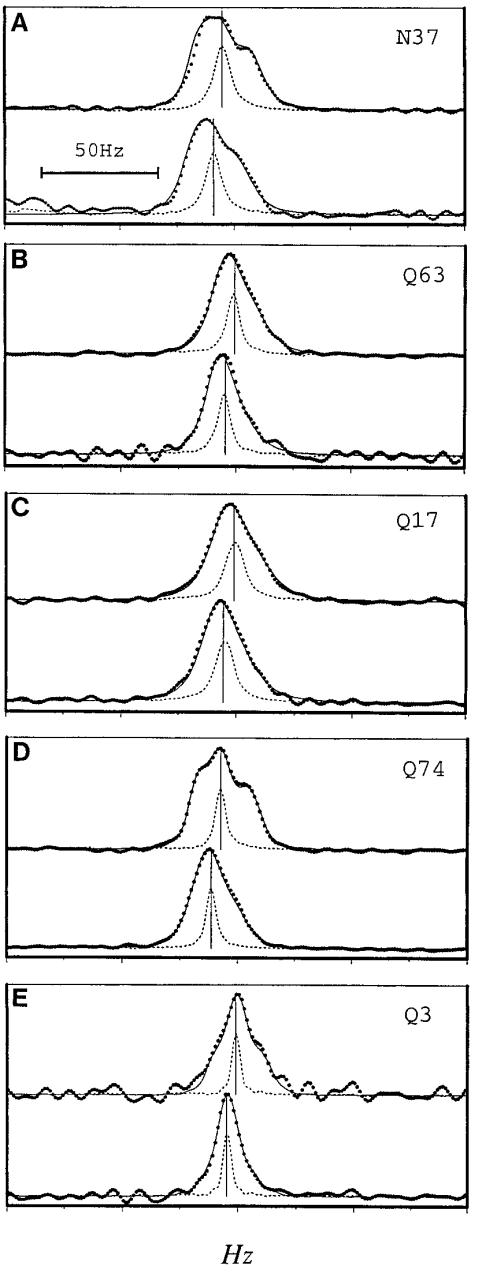

FIG. 7. Experimental cross sections parallel to F_1 at the ^{15}N frequency, corresponding to the ^1H resonances from the unassigned isotopomers Z-1-d and E-1-d, scalar coupled to ^2H, recorded from the protein F1-G. The experimental data were obtained using the pulse sequence in Fig. 5A and comprised 128 complex points, dwell time 860 μs, which were apodized with a line broadening of -4 Hz and zero filled three times prior to Fourier transformation. The ^{15}N spectra are from residues (A) N37, (B) Q63, (C) Q17, (D) Q74, and (E) Q3. Each diagram contains the experimental $^{15}N-^2H$ coupled data (filled circles) and a simulation (solid line). The dashed line is the experimental data resulting from applying ^2H and ^1H decoupling during the t_1 evolution period (these data are displayed with an arbitrary vertical scale). The vertical solid line is the first moment of the simulated lineshape. The first moment was defined as $\Sigma iA_i/\Sigma A_i$, where A_i is the amplitude of point i. The major and minor tick marks are at 50 and 25 Hz respectively. For the simulated lineshapes, the fixed parameters were as defined in the legend to Fig. 5. The variables which are necessary and specific for each residue are shown in Table 2. In all cases, the resonance offset used for the simulations was obtained from the fully (^1H and ^2H) decoupled data set.

that the D_E deuteron may be involved in a slightly stronger hydrogen bond than the D_Z deuteron. Very similar ^2H and ^{15}N spectral characteristics are observed if the amino acid is changed to glutamine. Using a similar approach for the analysis of ^{15}N lineshape data, assuming isotropic motion, the values found for the quadrupole coupling constants of the D_Z and D_E deuterons are shown in Table 1.

In aniline derivatives, the magnitude of the $^2\Delta^{13}C(D)$ isotope shifts have been correlated to hydrogen-bond strength (*59*). Both the $^1\Delta^{15}N(D)$ and the $^2\Delta H(D)$ isotope shifts are observed to be largest (although in opposite directions) for the E-1-d isotopomer. Whether these particular isotope shifts correlate with H-bond energy in this type of primary amide is not established.

The ^{15}N and ^1H spectral regions corresponding to all the resonances from the asparagine and glutamine side chains of the protein F1-G are shown in Fig. 6. A stereospecific assignment for the H_E and H_Z ^1H resonances was not attempted because of the uncertainty in the contributions to the observed chemical shifts of these resonances from nearby aromatic, carbonyl, or charged groups. ^{15}N lineshapes from residues N37, Q63, Q17, Q74, and Q3 recorded from a sample of the protein F1-G in an equimolar mixture of H_2O/D_2O are shown in Fig. 7, and quite asymmetric lineshapes can be observed for some of these resonances. In each diagram, the ^{15}N resonance correlated to the ^1H resonance at high frequency is the lower trace.

As a restraint on the motional parameters necessary to fit these data, an experimental measurement of the $^{15}N-^1H$ NOE was made for the asparagine and glutamine side chains from a sample of F1-G in a solvent ratio H_2O/D_2O of 95%/5%, at ^{15}N frequencies of 76 and 50 MHz. The experimental NOE values for the side-chain ^{15}N resonances of residues N37, Q63, Q17, Q74, and Q3 are shown in Table 2. For all of the asparagine and glutamine residues in F1-G, the side-chain $^{15}N-^1H$ NOE values were found to either have the same value, within an experimental error of ± 0.05, or increase as the ^{15}N frequency increased. For the simple Lipari–Szabo model, using an isotropic rotational correlation time, τ_r, of 7.2 ns, these observations are only consistent if 10 ps $> \tau >$ 300 ps independent of values for S^2. If τ lies within the range 10 to 300 ps, the NOE is predicted to significantly decrease with increasing ^{15}N frequency. Three of the five residues chosen as examples (N37, Q63, and Q17) probably have similar motional characteristics as judged by the comparable $^{15}N-^1H$ NOE data, whereas the two remaining residues were found to have smaller NOE values, presumably reflecting increasing mobility.

TABLE 2

Experimental ^{15}N-^{1}H Nuclear Overhauser Enhancements, η, for Some of the Asparagine and Glutamine Side Chains from the Protein F1-G Measured at Field Strengths of 11.7 and 17.6 T, Quadrupole Coupling constants, $e^2Qq/\hbar$, Derived from Simulations to the ^{15}N Lineshapes Shown in Fig. 7, the Order Parameter S^2, and τ Used in the Simulations

			$e^2Qq/\hbar$ (kHz)			
	η (11.7 T)	η (17.6 T)	a	b	S^2	τ (ps)
N37	0.30	0.45	175	155	0.85	350
Q17	0.35	0.45	215	195	0.83	350
Q63	0.25	0.36	220	210	0.78	500
Q74	−0.02	0.04	190	150	0.70	350
Q3	−1.39	−1.03	290	225	0.12[a]	360[a]

Note. The lower trace in each diagram (A–E) of Figure 7 is associated with the quadrupole coupling constant in column a.

[a] For residue Q3, the extension to the Lipari–Szabo model of Clore *et al.* (*60*) was used where S_s^2, S_f^2, and τ were 0.3, 0.4, and 360 ps, respectively, and $S^2 = S_s^2 \times S_f^2$.

The values of $e^2Qq/\hbar$ estimated from the simulations are shown in Table 2. For all the simulations, the asymmetry parameter of the electric-field-gradient tensor was assumed to be small enough that it could be neglected. These values for the quadrupole coupling constants have fairly large errors because of the relatively large number of input parameters and assumptions necessary for the simulations. The quadrupole coupling constants combined with the motional parameters S^2 and τ predict ^2H T_1 and T_2 values (B_0 = 17.6 T) in the range of 9.3 to 21.6 ms and 0.7 to 3.2 ms respectively. The composite parameter $[10\pi T_1(^2H)J_{ND}]^2$ is predicted, from the simulations, to vary from about 16 to 90. It has been suggested (*31*) that whenever this parameter has a magnitude greater than about 50, a lineshape with fine structure which may also be asymmetric will be observed; this is in agreement with the experimental and simulated spectra shown in Fig. 7. The T_1 of a ^2H nucleus in a medium-sized protein will be expected to increase as the magnetic field strength increases so that these ^{15}N asymmetric lineshapes will only be observed at the highest currently available field strengths when τ_r is around 7 ns.

From the five simulated data sets, the dipolar–quadrupolar cross-correlation term is, in all cases, positive, which implies that the quadrupole coupling constants are also positive (with the assumption that $\theta_{DQ} = 0$). The effect of ^2H decoupling is to remove the contributions to ^{15}N relaxation from the ^2H quadrupole and the ($^{15}N-^2H$, ^{15}N) csa–dipolar mechanisms (*31*). A comparison of the ^2H-decoupled spectra with the ^2H-coupled spectra, Fig. 7, indicates that the chemical shift of the ^{15}N resonance in the presence of ^2H decoupling occurs at the mean frequency of the $^{15}N-^2H$ scalar-coupled multiplet. The mean frequency of the ^2H-coupled spectra can be calculated, if the S/N ratio is high enough, via the first moment (*61*) of the experimental spectrum or by using the simulated data to estimate the experimental first moment. The first moment of the simulated data coincides in all cases with the peak maximum of the fully (^1H and ^2H) decoupled spectra, to within the spectral digital resolution (1.2 Hz/point).

The magnitudes of $e^2Qq/\hbar$ estimated for each deuteron site from the spectra of residues N37 and Q74 are quite different from the sample of the free amino acids (see Tables 1 and 2), whereas, those from Q63, Q17, and especially Q3 are closer to the values found from a sample of the free amino acid glutamine. The motional parameters chosen for the simulated data adequately predict the experimental $^{15}N-^1H$ NOE measurements at both frequencies.

The differences observed for the values of $e^2Qq/\hbar$ and the lack of a direct correlation to the $^{15}N-^1H$ NOE data (N37, Q63, and Q17 have similar NOE values, but different quadrupole coupling constants were estimated for N37) could perhaps arise for several reasons. The variation in the quadrupole coupling constants of these three residues may indeed reflect aspects of hydrogen bonding. For instance, it has been noted previously that a departure from linearity in the hydrogen bond can produce a significant change in the ^2H quadrupole coupling constant (*62*). Furthermore, the magnitude of the ^2H electric-field gradient is determined largely by the charge distribution on the neighboring atoms (*63*). The simulations have indicated that the quadrupole coupling constant of the deuteron is positive. Consequently, a negative charge in some region along the ND axis, at the hydrogen-bond acceptor, should lead to a significant decrease in the electric-field gradient and to the observed quadrupole coupling constant. It is perhaps also possible that even if the CO of the amide group participates as the acceptor in a hydrogen bond the ^2H nucleus, because of the resonance hybrid nature of the OCN group, may be sensitive to the charge density on the

carbonyl oxygen. In addition, if the side chain is exchanging rapidly between several different sites and if each site gives rise to a different value for the quadrupole coupling constant, the observed value would reflect this exchange process. At this time, the definition of these side chains in the NMR structures of F1-G is not sufficient to distinguish these possibilities.

In this paper, we have demonstrated that it is possible to probe indirectly the environment of a ^{2}H nucleus in a protein, in a specific case, through the influence it has upon the transverse relaxation of a ^{15}N nucleus to which it is scalar coupled. Large differences have been observed for $e^2Qq/\hbar$ of the deuteron in the side chains of asparagine and glutamine residues of the protein F1-G, derived from simulations of experimental ^{15}N–^{2}H scalar-coupled lineshapes.

ACKNOWLEDGMENTS

This work is a contribution from the Oxford Centre for Molecular Sciences, which is supported by the BBSRC and MRC. The 750 MHz NMR instrument was partly funded by the LINK protein engineering project with industrial partners Zeneca and Oxford Instruments. One of us, T.K.M., thanks the INLAKS foundation for financial support.

REFERENCES

1. B. M. P. Huyghues-Despointes, T. M. Klingler, and R. L. Baldwin, *Biochemistry* **34,** 13,267 (1995).
2. N. Dekker, M. Cox, R. Boelens, C. P. Verrijzer, P. C. Van der Vliet, and R. Kaptein, *Nature* **362,** 852 (1993).
3. T. Yamazaki, S. M. Pascal, A. V. Singer, J. D. Forman-Kay, and L. E. Kay, *J. Am. Chem. Soc.* **117,** 3556 (1995).
4. R. X. Xu, J. M. Word, D. G. Davis, M. J. Rink, D. H. Willard, Jr., and R. T. Gampe, Jr., *Biochemistry* **34,** 2107 (1995).
5. S. S. Narula, R. W. Yuan, S. E. Adams, O. M. Green, J. M. Green, T. B. Philips, L. D. Zydowsky, M. C. Botfield, M. Hatada, E. R. Laird, R. J. Zoller, J. L. Karas, and D. C. Dalgarno, *Structure* **3,** 1061 (1995).
6. C. L. Perrin, *Science* **266,** 1665 (1995).
7. G. Gunnarsson, H. Wennerstrom, W. Egan, and S. Forsen, *Chem. Phys. Lett.* **38,** 96 (1976).
8. L. J. Altman, D. Laungani, G. Gunnarsson, H. Wennerstrom, and S. Forsen, *J. Am. Chem. Soc.* **100,** 8264 (1978).
9. A. Pardi, G. Wagner, and K. Wüthrich, *Eur. J. Biochem.* **137,** 445 (1983).
10. G. Wagner, A. Pardi, and K. Wüthrich, *J. Am. Chem. Soc.* **105,** 5948 (1983).
11. M. Weissman, *J. Chem. Phys.* **44,** 422 (1966).
12. L. G. Butler and T. L. Brown, *J. Am. Chem. Soc.* **103,** 6541 (1981).
13. R. Blinc and D. Hadzi, *Nature* **212,** 1307 (1966).
14. T. Chiba, *Bull. Chem. Soc. Jpn.* **43,** 1939 (1970).
15. M. J. Hunt and A. L. Mckay, *J. Magn. Reson.* **15,** 402 (1974).
16. B. Berglund, J. Lindgren, and J. Tegenfeldt, *J. Mol. Struct.* **43,** 179 (1978).
17. N. Karlsbeek, K. Schaumberg, and S. Larsen, *J. Mol. Struct.* **299,** 155 (1993).
18. U. Sternberg and E. Brunner, *J. Magn. Reson. A* **108,** 142 (1994).
19. N. J. Heaton, R. L. Vold, and R. R. Vold, *J. Am. Chem. Soc.* **111,** 3211 (1989).
20. W. Egan, G. Gunnarsson, T. W. Bull, and S. Forsen, *J. Am. Chem. Soc.* **29,** 4568 (1977).
21. L. M. Jackman, J. C. Trewella, and R. C. Haddon, *J. Am. Chem. Soc.* **102,** 2519 (1980).
22. R. Ludwig, J. Bohmann, and T. C. Farrar, *J. Phys. Chem.* **99,** 9681 (1995).
23. J. A. Pople, *Mol. Phys.* **1,** 198 (1957).
24. A. Abragam, ''The Principles of Nuclear Magnetism,'' Clarendon Press, Oxford, 1961.
25. R. K. Harris and N. C. Pyper, *Mol. Phys.* **20,** 467 (1971).
26. L. G. Werbelow, *J. Magn. Reson.* **67,** 66 (1986).
27. L. G. Werbelow, A. Allouche, and G. Pouzard, *J. Chem. Soc. Faraday Trans.* **83,** 871 (1987).
28. R. E. London, D. M. LeMaster, and L. G. Werbelow, *J. Am. Chem. Soc.* **116,** 8400 (1994).
29. S. Grzesiek and A. Bax, *J. Am. Chem. Soc.* **116,** 10,196 (1994).
30. L. G. Werbelow and R. E. London, *J. Chem. Phys.* **102,** 5181 (1995).
31. N. Murali and B. D. Nageswara Rao, *J. Magn. Reson. A* **118,** 202 (1996).
32. R. R. Ernst, G. Bodenhausen, and A. Wokaun, ''Principles of Nuclear Magnetic Resonance in One and Two Dimensions,'' Clarendon Press, Oxford, 1987.
33. C. N. Banwell and H. Primas, *Mol. Phys.* **6,** 225 (1963).
34. C. E. M. Fouques and L. G. Werbelow, *Can. J. Chem.* **57,** 2329 (1979).
35. J. McConnell, ''The Theory of Nuclear Magnetic Relaxation in Liquids,'' Cambridge Univ. Press, Cambridge, 1987.
36. G. Lipari and A. Szabo, *J. Am. Chem. Soc.* **104,** 4546 (1982).
37. C. A. Michal, J. C. Wehman, and L. W. Jelinski, *J. Magn. Reson. B* **111,** 31 (1996).
38. J. Herzfield, J. E. Roberts, and R. G. Griffin, *J. Chem. Phys.* **86,** 597 (1987).
39. B. O. Smith, A. K. Downing, T. J. Dudgeon, M. Cunningham, P. C. Driscoll, and I. D. Campbell, *Biochemistry* **33,** 2422 (1994).
40. B. O. Smith, A. K. Downing, P. C. Driscoll, T. J. Dudgeon, and I. D. Campbell, *Structure* **3,** 823 (1995).
41. N. R. Krishna, K. P. Sarathy, D. Huang, R. L. Stephens, J. D. Glickson, C. W. Smith, and R. Walter, *J. Am. Chem. Soc.* **104,** 5051 (1982).
42. N. Soffe, J. Boyd, and M. Leonard, *J. Magn. Reson. A* **116,** 117 (1995).
43. C. L. Perrin, J. D. Thoburn, and A. J. Kresge, *J. Am. Chem. Soc.* **114,** 8800 (1992).
44. M. Wolfsberg, *Acc. Chem. Res.* **20,** 449 (1972).
45. G. Jansco and W. A. van Hook, *Chem. Rev.* **74,** 689 (1974).
46. K. B. Schowen and R. L. Schowen, *Methods Enzymol.* **87,** 551 (1982).
47. A. G. Redfield and S. Waelder, *J. Am. Chem. Soc.* **101,** 6151 (1979).
48. P. E. Hansen, *Prog. NMR Spectrosc.* **20,** 207 (1988).

49. G. Fraenkel, Y. Asahi, H. Batiz-Hernandez, and R. A. Bernheim, *J. Chem. Phys.* **44,** 4647 (1966).

50. M. Shporer and A. Loewenstein, *Mol. Phys.* **15,** 9 (1988).

51. S. N. Loh and J. L. Markley, *Biochemistry* **33,** 1029 (1994).

52. R. R. Vold and R. L. Vold, *Adv. Magn. Opt. Reson.* **16,** 85 (1991).

53. J. Boyd, *J. Magn. Reson. B* **107,** 279 (1995).

54. V. A. Daragen and K. H. Mayo, *J. Phys. Chem.* **98,** 10,949 (1994).

55. J. Garcia de la Torre and V. A. Bloomfield, *Q. Rev. Biophys.* **14,** 81 (1981).

56. G. Kartha and A. de Vries, *Nature* **192,** 862 (1961).

57. A. Bax, M. Ikura, L. E. Kay, D. A. Torchia, and R. Tschudin, *J. Magn. Reson.* **86,** 304 (1990).

58. L. E. Kay, P. Keifer, and T. Saarinen, *J. Am. Chem. Soc.* **114,** 10663 (1992).

59. J. Reuben, *J. Am. Chem. Soc.* **109,** 316 (1987).

60. G. M. Clore, A. Szabo, A. Bax, L. E. Kay, P. C. Driscoll, and A. M. Gronenborn, *J. Am. Chem. Soc.* **112,** 4989 (1990).

61. J. A. Pople, W. G. Schneider, and H. J. Bernstein, ''High Resolution Nuclear Magnetic Resonance,'' McGraw–Hill, New York, 1959.

62. L. G. Butler and T. L. Brown, *J. Am. Chem. Soc.* **103,** 6541 (1981).

63. L. C. Snyder, *J. Chem. Phys.* **68,** 291 (1978).